

Characteristics of recoil leaders as observed by LOFAR

B. M. Hare^{1,6,*} O. Scholten^{1,2} S. Buitink^{3,4} J. R. Dwyer⁵ N. Liu⁵ C. Sterpka⁵ and S. ter Veen⁶

¹*Kapteyn Astronomical Institute, University Groningen, Landleven 12, 9747 AD Groningen, Netherlands*

²*Interuniversity Institute for High-Energy, Vrije Universiteit Brussel, Pleinlaan 2, 1050 Brussels, Belgium*

³*Department of Astrophysics/IMAPP, Radboud University Nijmegen, Nijmegen 6500 GL, Netherlands*

⁴*Astrophysical Institute, Vrije Universiteit Brussel, Pleinlaan 2, 1050 Brussels, Belgium*

⁵*Department of Physics and Astronomy & Space Science Center (EOS), University of New Hampshire, Durham, New Hampshire 03824, USA*

⁶*Netherlands Institute for Radio Astronomy (ASTRON), Dwingeloo 9433 TA, Netherlands*



(Received 14 September 2022; accepted 11 January 2023; published 31 January 2023)

Lightning dart leaders and recoil leaders are current pulses that propagate along previously established lightning channels reionizing the channel. They are poorly understood since it is not known how a previously ionized channel can undergo dielectric breakdown multiple times. In this work we investigate five recoil leaders on two different channels using lightning observations of the LOFAR radio telescope in vhf (where we observe 30–80 MHz) using our TRI-D interferometric imaging algorithm. We show that while recoil leaders do slow down over time on average, they can also clearly accelerate. In addition, the vhf power emitted by the recoil leader is closely correlated with speed. We also investigate the vhf-emitting width of the recoil leaders and show that it is thinner than our meter-scale resolution. This shows that recoil leaders have significant streamer activity in their channel core or at most very inner region of the corona sheath, and that there is either very little, or weakly vhf-emitting, streamer activity in the majority of the corona sheath. Finally, we show that recoil leaders can have small microsecond-scale fluctuations in emitted vhf power that can occur in the same spot across subsequent recoil leaders on the same channel, demonstrating that recoil leader propagation is affected by small-scale channel geometry.

DOI: [10.1103/PhysRevD.107.023025](https://doi.org/10.1103/PhysRevD.107.023025)

I. INTRODUCTION

After lightning initiates there are positive and negative plasma channels, called leaders, that propagate through the thundercloud seeking regions of opposite charge and sometimes even connecting to ground. When a leader propagates through a region of air, a series of complex and poorly understood processes break down the air into a hot and conducting plasma. Negative leaders have a tendency to propagate in discrete jumps that are called “steps.” Near ground these jumps tend to be about 10 m long and about 10 μ s in duration, but the scale is highly altitude dependent [1–3]. Negative leaders have two major spatial regions, an inner highly conducting core centimeters in diameter and a poorly conducting corona sheath that stores the charge. The exact radius of the corona sheath in leaders propagating kilometers above ground has never been measured, but we expect it be about the same size as the step length; thus, around 10 m and larger. This is supported by optical observations of a leader at 10 km altitude that had a streamer corona around 200 m in length, as well as 200 m step lengths [3,4]. The path of these

negative leaders is known to be extremely tortuous and fractal-like over a large range of scales. However, it is reasonable to expect the nature of leader tortuosity to change around the 10 m scale (the stepping length), but this lower-limit of leader tortuosity has not been observed.

Eventually, as the channel cools down, it somehow becomes unstable [5] and the lightning will exhibit strong current pulses that start on the positive leader and propagate backwards (in a negative direction) along the previously established lightning channel with speeds on the order of 1×10^7 m/s and transporting negative charge in a direction away from the positive leader tip [1]. During propagation these pulses emit light and broadband radio, and are thus considered to be another type of leader despite the fact they do not establish any new channel. Sometimes these pulses propagate a significant distance and can pass all the way through the positive leader channel and onto the negative leader channel. If the current pulse propagates so far that it connects to the ground, then it is referred to as a dart leader. However, the lightning community is divided in how to refer to this phenomenon if it does not reach ground. Common names include K leaders, negative retrograde breakdown, and recoil leaders [6]. In this work we prefer the term “recoil leader” since it is both short and somewhat

*b.h.hare@rug.nl

describes the physics of the phenomena (in the sense that the current pulse “recoils” in the opposite direction of the positive leader that it initiates on).

The physics of recoil leader propagation is very poorly understood. It has been observed that recoil leaders can propagate very smoothly, but sometimes they also exhibit a stepping behavior like negative leaders [1]. Though it is not at all clear what properties influence a recoil leaders behavior, for example if there is a discrete phase transition between stepping and smooth propagation, or if there is a continuous range between the two behaviors. It has also been observed that recoil leaders can slow down as they propagate [6–8].

While a recoil leader resembles a charge pulse that travels along a poor conductor, it cannot be described by a transmission line since the propagation velocity is too small [9]. We know that recoil leaders exhibit significant dielectric breakdown due to the fact they emit vhf (30–300 MHz) radio radiation, but it is not understood how a previously established channel can undergo dielectric breakdown multiple times. It has been proposed that dart leaders can be thought of as a guided soliton that propagates by, and speed is governed by, electron impact and thermal ionization [6]. As the soliton propagates it loses energy, thus ionizing the plasma more slowly, and thus it propagates more slowly. However, [6] was unable to specify what form this energy takes, the mechanism by which that energy is stored or lost, or the role of electron impact and thermal ionization.

Our group has discovered a lightning phenomenon we call needles, which are small (< 100 m long) structures perpendicular to positive leader channels, possibly inside the positive leader corona sheath [10]. We speculated that perhaps these needles could enhance leader instability and thus be a major cause of recoil leaders. Subsequent work by other groups claimed to find no connection between recoil leaders and needles [11,12]. However, a recent detailed work by our group showed that needle activity is very regularly followed by recoil leaders and a cessation of needle activity [13].

Therefore, in this work we use the LOFAR radio telescope [14,15] to investigate recoil leaders. Not just because they are a fascinating phenomenon that is poorly understood, but also because they could prove to be very useful probes into the structure of the lightning plasma channel and be used to shed light on other lightning phenomena. In this work we show that recoil leaders can have meter-level thin vhf emission, where meter-level tortuosity recoils speed and vhf power is correlated. Finally, while recoil leaders generally slow-down as they propagate, they can also speed up as well.

II. LIGHTNING FLASH AND INITIAL ANALYSIS

A. LOFAR

In this work we use data collected by the LOFAR radio telescope, which has stations all over Europe. In this work

we use the 36 Dutch LOFAR stations. From each station we use data from 6 LBAs (low band antennas), which operate in the 30–80 MHz regime. LOFAR continuously buffers antenna voltages on to a circular antenna buffer, and when a lightning flash is detected this buffer is frozen and two seconds of data around the lightning flash are read to disk [14].

After recording, we pass our data through an analysis chain [15–17]. The primary stages consist of RFI (radio frequency interference) cleaning where we detect human radio stations via their phase stability, and remove them, and a timing calibration. After these steps we image our data to find the location of the lightning vhf radio sources.

B. Imaging

We use our recently developed 3D interferometric technique we call TRI-D [17]. The technique is derived and explained in detail in [17]. In summary, at each antenna (with index a) we measure the complex-valued electric fields $\vec{E}_a(t)$; which is the measured antenna voltages with the antenna response removed, including the fact that $\vec{E}_a \cdot \hat{r}_a = 0$. Where \hat{r}_a is the unit vector pointing from antenna a to the source region. For notational simplicity, $\vec{E}_a(t)$ also has all geometric and calibration time delays removed (i.e., $t = 0$ is always the same time at the source independent of the antenna index a). These antenna voltages can be summed together to extract the 3D dipole moment at the source location;

$$A\vec{p} = \sum_a \vec{E}_a w_a / R_a, \quad (1)$$

where \vec{p} is the time/frequency dependent 3D complex-valued dipole moment at the source region. w_a is a set of weights per antenna. The analysis is not sensitive to how w_a are chosen, and we choose w_a to be inversely proportional to the antenna noise. R_a is the distance from antenna to source region. A is a 3×3 matrix that represents the layout of the antennas;

$$A_{ij} = \sum_a (\delta_{ij} - \hat{r}_{a,i} \hat{r}_{a,j}) w_a / R_a^2, \quad (2)$$

where δ_{ij} is the Kronecker delta. Note that as long the antennas are sufficiently spread around the lightning flash, then A is invertible.

During our interferometric procedure we pick a rectangular region in the sky and voxelate it with 1 m sized voxels. This space is typically around 100 m per side, limited by computer memory. We then find $\vec{p}(t)$ for each voxel using Eq. (1), for the length of time we want to image (typically up to 300 μ s). This 4D cube is then chopped into 100 ns duration time slices, and for each time slice the voxel with maximum total intensity ($I = |\vec{p}|$ summed over the 100 ns time slice) is chosen as the source location.

Since LOFAR's background noise is dominated by the galactic background [18], we can normalize our raw data relative to the galactic background radio power so that the units of our intensity are in terms of the galactic background (gb). A source with an intensity of 1 gb is such that an antenna 1 km away receives the same energy (integrated over the 100 ns window) from the lightning radio source as it does the galactic background. Note that if we apply our imager to a region of empty space at the same time of the lightning flash, then we find that the third quantile of the resulting amplitude spectrum is about 20 gb. Finally, we apply our beamforming to multiple recoil leaders by placing many imaging hypercubes over the 4D trajectory of the recoil leader and combining their results. After imaging we removed sources that had an intensity below 20 gb.

C. Resolution

Estimating the location accuracy of the located sources is challenging. In [17] we attempted to estimate the location accuracy by simulating the emission from a dipole point source and injecting background noise. We simulated two scenarios: one with a single point source and background noise chosen so that the signal-to-noise ratio is 1:1 on a reference antenna on LOFAR's core, and in the second scenario we simulated a cloud of 1000 point sources that had a random Gaussian profile with a standard deviation of 20 m in space and 0.4 μ s in time. The result is a single point source with large background noise typically has a jitter less than 1 m. However, in a worse-case scenario, if the pulse falls on the edge between two slices it can have a location jitter of about 10 m in the radial direction. However, the 20 m width point source cloud has an imaged width of about 40 m in the radial direction. These results indicate the difficulty in quantifying the true location accuracy. The contribution due to background noise is minimal and perhaps quantifiable. However, the major contribution to location error is due to multiple interfering point sources, which is very difficult to understand and quantify. The conclusion is that it is relatively easy to provide an upper limit to the size of lightning vhf phenomena, as we will do in this work. However, showing that an imaged vhf spread is truly physical, rather than instrumental, is difficult. These simulations do provide one clue to distinguish instrumental from physical source spread. Instrumental spread is primarily in the radial direction from the LOFAR core, where the lightning physical vhf spread should be independent of the radial direction.

D. The lightning flash

The event we used in this work occurred at 21:03:06 UTC on April 24, 2019. It consisted of two or three close lightning flashes (in one case it is difficult to tell if there is a new flash or continuation of a previous flash). The entire

lightning flash, shown in Fig. 1, was imaged with our impulsive imager [19], which is a computationally efficient technique that does not produce quite as high-quality images as our TRI-D interferometry. Figure 1 also highlights five recoil leaders (A, B, C and G, H) that we imaged with our TRI-D interferometry. Recoils A, B, and C were subsequent recoil leaders along the same channel, and recoils G and H were also subsequent recoils on a channel different from that of recoils A, B, and C. We choose to image these five recoils in order to explore recoils in different locations, as well as recoils along same channels to explore conditioning. These five recoil leaders are very typical of recoil leaders seen by LOFAR, and they are very similar to each other in terms of spatial structure, speed, and radio intensity (as will be shown during this work). Therefore we expect that the properties of these five recoil leaders should be relatively representative of common recoil leader behavior. Figure 2 shows an enlargement of recoils H, G, and A, B, C. In both Figs. 1 and 2 the gray dots are sources located by the impulsive imager and colored dots are sources located by the TRI-D beamformer. Both Figs. 1 and 2 also contain recoil leaders (other than H, G, or A, B, C) that we have not investigated in this work.

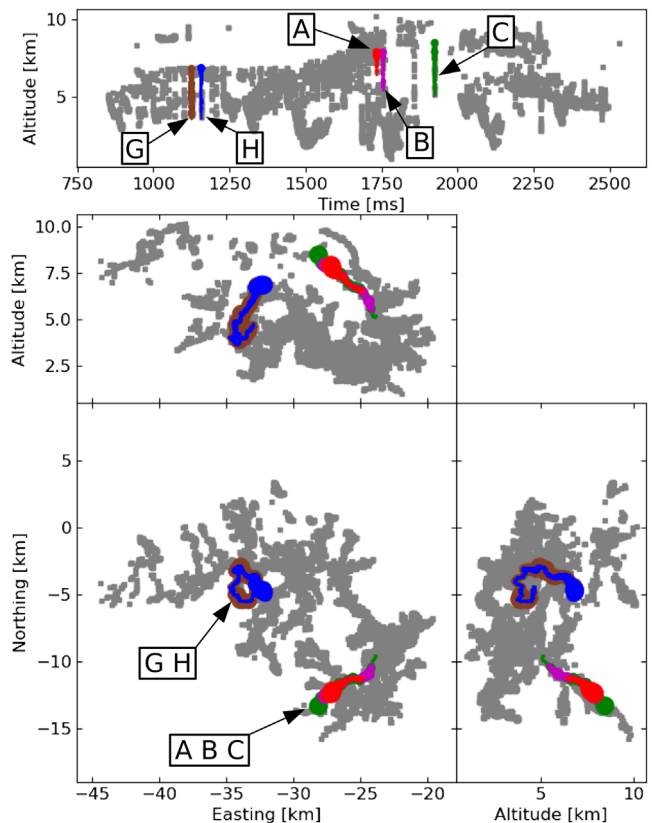


FIG. 1. Entire event with five recoils highlighted. Gray dots are sources located by the impulsive imager and colored dots are recoil leader sources located by the TRI-D beamformer for the recoils under consideration in this work.

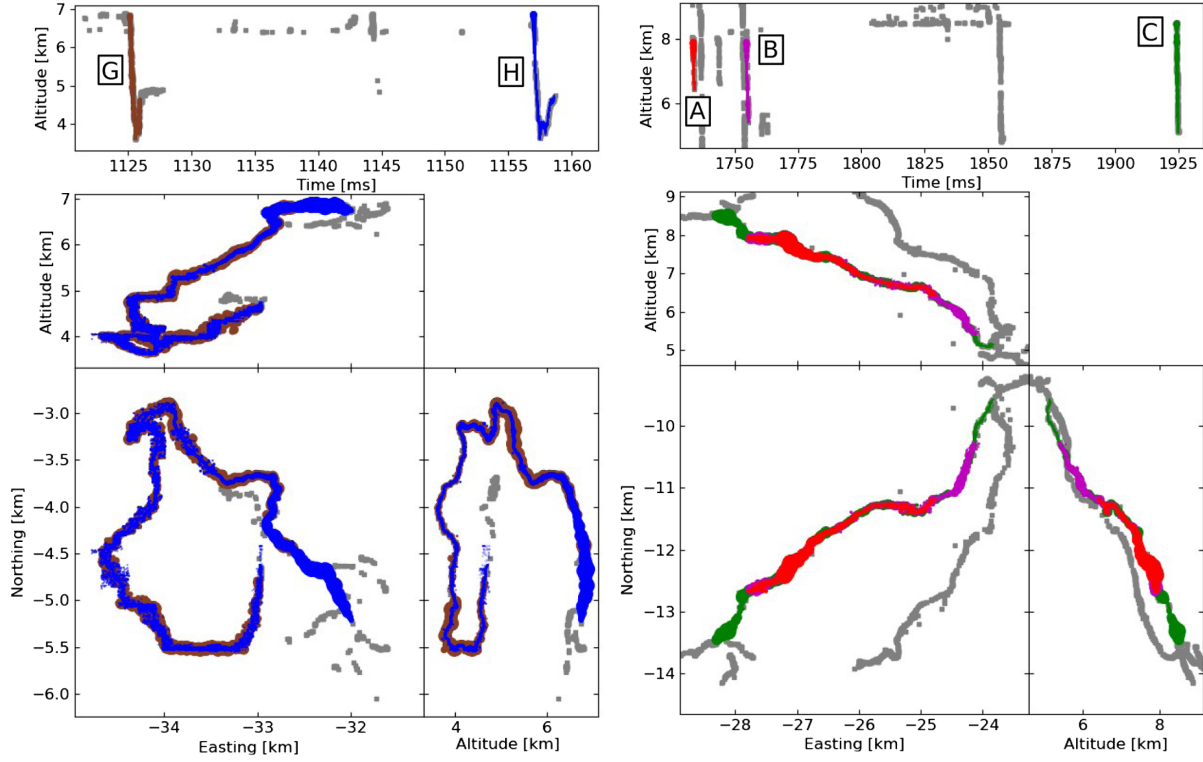


FIG. 2. Enlargement of recoils G and H (left), and recoils A, B, and C (right). Gray dots are sources located by the impulsive imager and colored dots are sources located by the TRI-D beamformer for the recoils under consideration in this work.

E. Spline fitting

In order to extract propagation speeds and analyze vhf width we fit smoothing splines to the vhf source locations. Since the majority of our location error is in the radial direction from the LOFAR core [17], we fit the 1D splines to the radial, azimuthal, and zenithal source coordinates (in a locally Cartesian coordinate system relative to the LOFAR core) vs time. The coordinate transformation given by

$$\begin{bmatrix} X_r \\ X_\theta \\ X_\phi \end{bmatrix} = \begin{bmatrix} \sin \bar{\theta} \cos \bar{\phi} & \sin \bar{\theta} \sin \bar{\phi} & \cos \bar{\theta} \\ \cos \bar{\theta} \cos \bar{\phi} & \cos \bar{\theta} \sin \bar{\phi} & -\sin \bar{\theta} \\ -\sin \bar{\phi} & \cos \bar{\phi} & 0 \end{bmatrix} \begin{bmatrix} X_e \\ X_n \\ X_a \end{bmatrix}, \quad (3)$$

where X_r , X_θ , X_ϕ are the radial, azimuthal, and zenithal coordinates, X_e , X_n , X_a are the easting, northing, and altitude coordinates; and $\bar{\theta}$, $\bar{\phi}$ are the average zenithal and azimuthal angle averaged over 100 μs (all sources per spline).

A spline is fit over each section of 100 μs duration for all recoil leaders. Each spline consists of a set of cubic polynomial knots, where the parameter controlling the amount of smoothing is the ratio between number of knots and vhf sources. Note that we used the same knot locations for the radial, azimuthal, and zenithal splines. Picking the number of knots is challenging, as there should be enough

knots to match channel tortuosity but not so many that the splines overfit the source data and are heavily influenced by source scatter. This difficulty is illustrated by Fig. 3, which shows small sections along two recoil leaders B and H. These two sections are fairly typical of recoil leaders that we have imaged. Figure 3 shows that these two recoil sections are very thin, as seen in vhf, significantly less than 10 m wide as the majority vhf sources in Fig. 3 are within 5 m of the spline. In addition Fig. 3 shows the meter-scale tortuosity of the recoil leaders. Two examples of meter-scale tortuous kinks are indicated in Fig. 3 with black arrows. These features are general, and we see that recoils can have smooth segments but tend to have meter-scale bends and kinks in their channel. As a result, it is challenging to develop a technique that reliably produces a spline that is smooth enough to average over vhf scatter, but flexible enough to match the meter-scale channel tortuosity. It should be noted that we have checked the persistence of the channel tortuosity over subsequent recoils, and have found that later recoil leaders pass over the same track as earlier recoil leaders.

In order to properly choose the number of knots, Fig. 4 shows the standard deviation of the difference between source (\bar{X}^{source}) and spline (\bar{X}^{spline}) locations in the radial, azimuthal, and zenithal directions [i.e., $\sigma(X_r^{\text{source}} - X_r^{\text{spline}})$, $\sigma(X_\theta^{\text{source}} - X_\theta^{\text{spline}})$, and $\sigma(X_\phi^{\text{source}} - X_\phi^{\text{spline}})$] as a function of number of knots (normalized by number of sources) for two

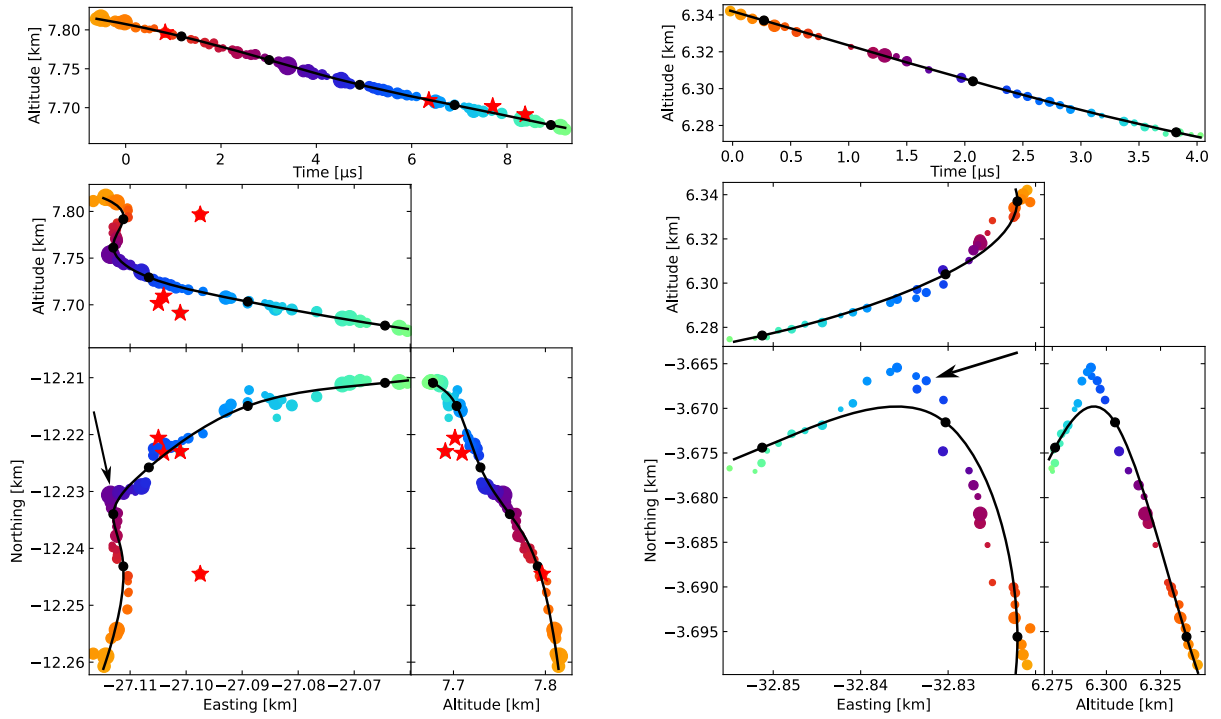


FIG. 3. Enlargement small-scale structure of two recoil sections from recoil leaders B (left) and H (right) accordingly. Dot size shows vhf source intensity. Color indicates time. T_0 in the left panel is $T = 1754.69$ ms in Figs. 1 and 2. T_0 in the right panel is $T = 1157.06$ ms in Figs. 1 and 2. Black line show final spline fit, black show spline knot locations, and red stars show sources excluded from the spline fit [4 in plot bounds for B (left), none in plot bounds for H (right)]. In both panels an example of meter-scale channel tortuosity is indicated by a black arrow.

100 μ s sections of recoil leaders H and B. Figure 4 shows that the largest scatter is in the radial direction as expected, and that the standard deviation starts large and drops quickly as the number of knots increases, eventually converging to a stable channel width. The number of knots should be chosen to be in this converged region. We choose to use 0.05 knots per source (20 sources per knot). We have checked that this produces well-fitting splines by eye and that the results of this work do not change if we choose 10 or 40 sources per knot.

After choosing the number of knots we excluded outlier sources. This was done by excluding the source farthest from the spline and then refitting the spline, repeating until all sources were within 10 m of the spline. We choose 10 m as Fig. 3 shows that the actual channel width is much smaller than 10 m. Note that this is in contrast to Fig. 4, which shows that the standard deviation of the data can be larger than 10 m. Figure 4, however, is dominated by scatter of poorly located sources which can be seen by the fact that the standard deviation is largest in the radial direction in

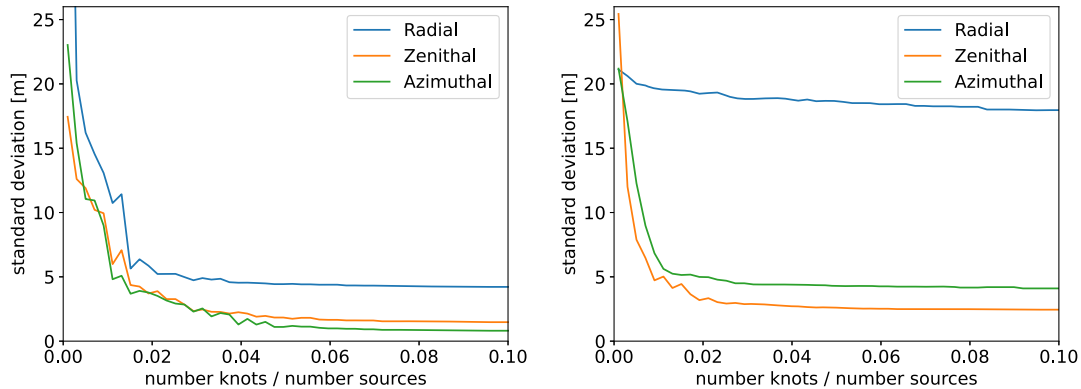


FIG. 4. Standard deviation of difference between spline and source locations for two 100 μ s sections of recoil leaders H (left) and B (right), as a function of number of knots normalized by number of vhf sources.

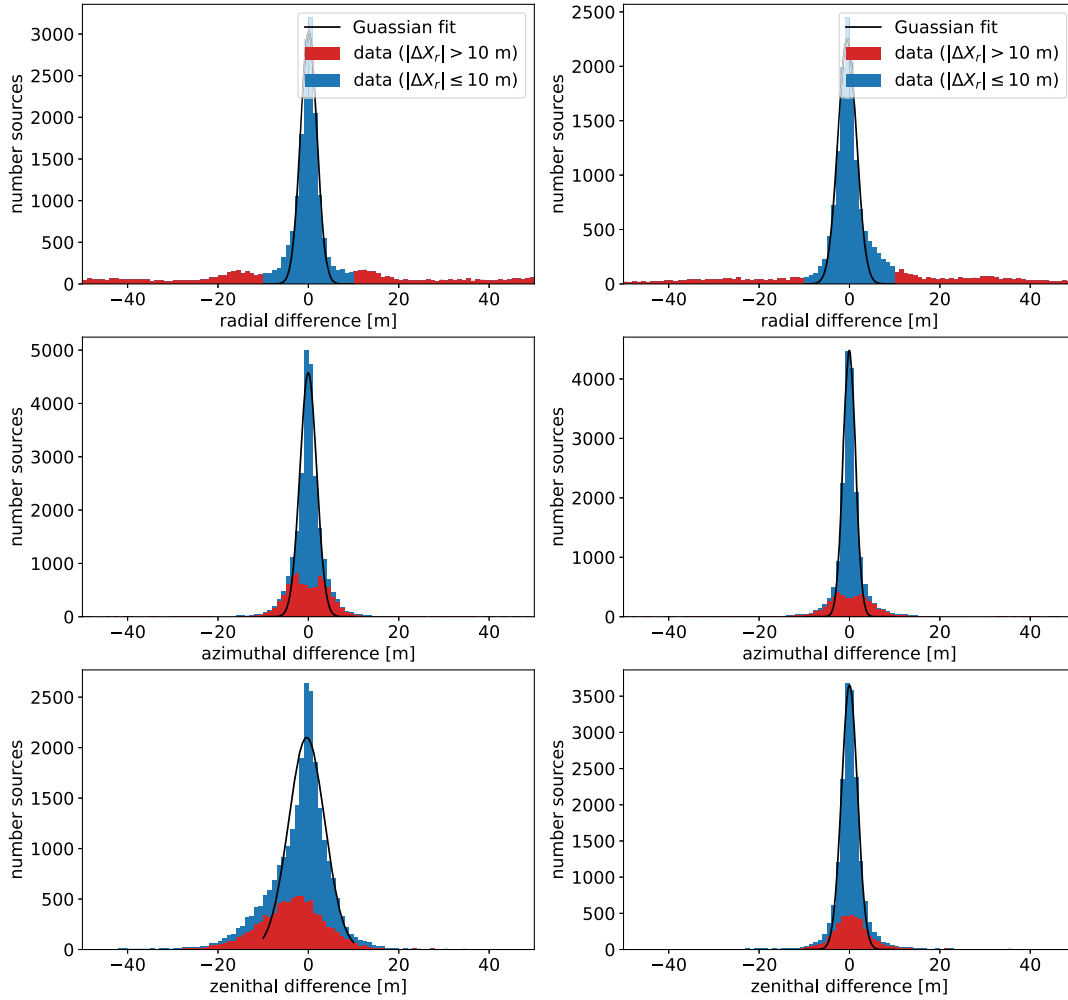


FIG. 5. Histogram of difference between source and spline locations in radial, azimuthal, and zenithal coordinates [as defined by Eq. (3)]. Height of bin shows number of sources in bin, and fraction of bin that is red indicates fraction of sources in that bin that has a displacement from the spline greater than 10 m in the radial direction. A black line shows a Gaussian function fit to the bins within 10 m, the resulting widths shown in Table I.

Fig. 4, and will be more evident from Fig. 5 below. Figure 3 also shows the final resulting spline fit, and the sources excluded from the spline are indicated by red stars. Note that the excluded sources were only removed from the spline fitting, and are still included in all subsequent analysis. Figure 3 shows that the spline resulting from this sophisticated procedure can match general channel tortuosity, but still struggles to truly match the smallest meter-scale tortuosity as evidenced by the channel kinks indicated by the arrows in Fig. 3.

Figure 5 shows histograms of differences between source and spline coordinates in the radial, azimuthal, and zenithal coordinates as defined by Eq. (3). The histograms include all the sources in the G and H recoil leaders and all the sources in the A, B, and C recoil leaders; where the height of each bin shows the total number of sources in the bin and the fraction of the bin that is red versus blue indicates the fraction of sources that have a radial direction difference

greater than 10 m ($|\Delta X_r| > 10$ m). We have investigated the distributions of source location scatter for each recoil individually, and they are very similar to the aggregate distributions shown in Fig. 5. Figure 5 shows that the source scatter in the radial direction contains two primary components; a tall sharp normally distributed component with meter-level standard deviation, and a low amplitude broad background. Based on our experiences imaging various Monte Carlo simulations [17] (discussed in Sec. II C), the sharp spike in Fig. 5 is constant with source location error due to normally distributed background noise, and the broad background error is due to lightning radio sources interfering with each other. In addition both components are broadened by the spline not entirely fitting sharp bends in the leader channel. Figure 5 validates our decision to exclude sources more than 10 m away in the spline fit, as 10 m is a good demarcation distance between small source location errors due to background noise and

TABLE I. Standard deviation widths, with 1 standard deviation error bars, of the Gaussian function fits in Fig. 5.

Coordinate	Recoils G, H	Recoils A, B, C
Radial	1.80 ± 0.09 m	2.03 ± 0.12 m
Azimuthal	1.84 ± 0.12 m	1.37 ± 0.06 m
Zenithal	3.99 ± 0.30 m	1.75 ± 0.06 m

the large source location errors due to multiple interfering sources. Figure 5 also shows a Gaussian function fitted to the central sharp spike (using the histogram bins that are within ± 10 m), allowing us to extract the width of the central component of the source scatter, results are in Table I. Note that the broad background in Fig. 5 is the reason behind the large radial standard deviations in Fig. 4. It is interesting that the distribution of scatter in the zenithal direction of recoil leaders G and H differs significantly from the other distributions. It has an asymmetric shoulder towards the negative values that primarily consists of sources that have also have a large radial scatter. This shows that there is some correlation between radial and zenithal location errors and that sources with a large radial error tend to have somewhat smaller zenithal location. While this is an interesting observation about our imaging technique, it should not affect the results of this work other than inflating the Gaussian width for this coordinate in Table I. This effect is probably visible in recoil leaders G and H, and not A, B, and C, since G and H have more sources with large scatter in the radial direction ($|\Delta X_r| > 10$ m). The conclusion from Fig. 5 and Table I is that the scatter of the located sources around the spline fit is entirely explained by the spline not fitting meter-level tortuosity and by source location error estimated from monte carlo simulations [17]. Thus, the vhf-emitting width of these five recoil leaders must be smaller than LOFARs resolution.

III. RESULTS

A. Propagation speed versus intensity

Using LOFAR data and our spline we can explore how properties of the recoil leaders change over their lifetime. To pursue this, we first calculated the speed vs time for each recoil by taking the derivative of the spline position vs time. Then we chopped each recoil leader into $10 \mu\text{s}$ duration bins, and for each bin calculated the average, 16th and 84th percentile of the speeds (corresponding to $\pm 1\sigma$ if speeds were normally distributed), distance along the leader, and reconstructed power averaged over the bin ($\sum_i I_i / \Delta T$, where I_i is source intensity and ΔT is the duration of the bin, $10 \mu\text{s}$). Figure 6 shows average power, speed, and a log-linear ratio of the two vs time from the start of the recoil leader. Figure 7 is the same, except as a function of distance along the channel. The log-linear ratio will be motivated and discussed further below.

These figures show that vhf power and speed have complex structure. In general, speed and power decrease over distance/time. However, surprisingly, the power and speed can also drastically increase. For example, recoil G has a sharp increase in speed and vhf power near the end of its propagation ($T = 750 \mu\text{s}$, $D = 10$ km). Recoil H, over the same channel, has a different structure but shows a bump in speed and intensity at $T = 250 \mu\text{s}/D = 6$ km. In addition, recoils A and B both accelerate significantly immediately after they start propagating.

One question is if these fluctuations in speed and power are due to recoil propagation physics (e.g., recoil wave losing or gaining charge), or due to channel structure (e.g., width or level of ionization). Comparison of Figs. 6 and 7 show that the speed of subsequent recoils tends to line-up better with respect to distance along the channel than time from start. Primarily, recoils A and B reach their peak speed/power at the same distance but different time from start. This strongly implies that much of the fluctuations in speed/power are due to channel geometry. However, there are also significant differences between subsequent recoils. Namely, recoil C has different structure from A and B, and recoil G and H are different. These differences could be due to changes in the conductivity or level of ionization of the channel.

It is surprising that the log of power and speed have similar structure in each recoil. This behavior motivates a comparison to an exponential relationship between the two:

$$P = K10^{V/Q}, \quad (4)$$

where P is the average power over time, V is the speed, and K and Q are constants that we found by numerically fitting $\log P$ and V , per recoil, with a line. The final values of K and Q are shown in Table II. Note that for recoil B we only fitted data from the first half of the recoil leader, as the relationship between P and V for recoil B changes significantly near $T = 410 \mu\text{s}$. A vertical black line in Figs. 6 and 7 indicate the time/location where we cut recoil B. To show the results, Figs. 6 and 7 plot $V/\log(P/K)$ vs time and distance respectively. If the power/speed relationship perfectly matches an exponential function, then $V/\log(P/K)$ would be exactly flat and equal to the fitted Q . Figures 6 and 7 show that $V/\log(P/K)$ is indeed very flat, and relatively similar for different recoil leaders, although distinctly larger for recoils G and H. It is about 8×10^6 m/s for recoils G and H, and varies between 5×10^6 to 8×10^6 m/s for recoils A, B, and C. Nevertheless, there are two major locations where the recoils clearly deviate from the exponential relationship. The first is at the end of recoil H, exactly where recoil H shows a sharp spike in I_{90}/P . In addition, as eluded above, recoil B shows a distinct change in its behavior in the middle of its propagation. Before $T = 410 \mu\text{s}/D = 7.2$ km, recoil B's $V/\log(P/K)$ is around 7×10^6 m/s, and afterwards recoil B's $V/\log(P/K)$ is around 4×10^6 m/s.

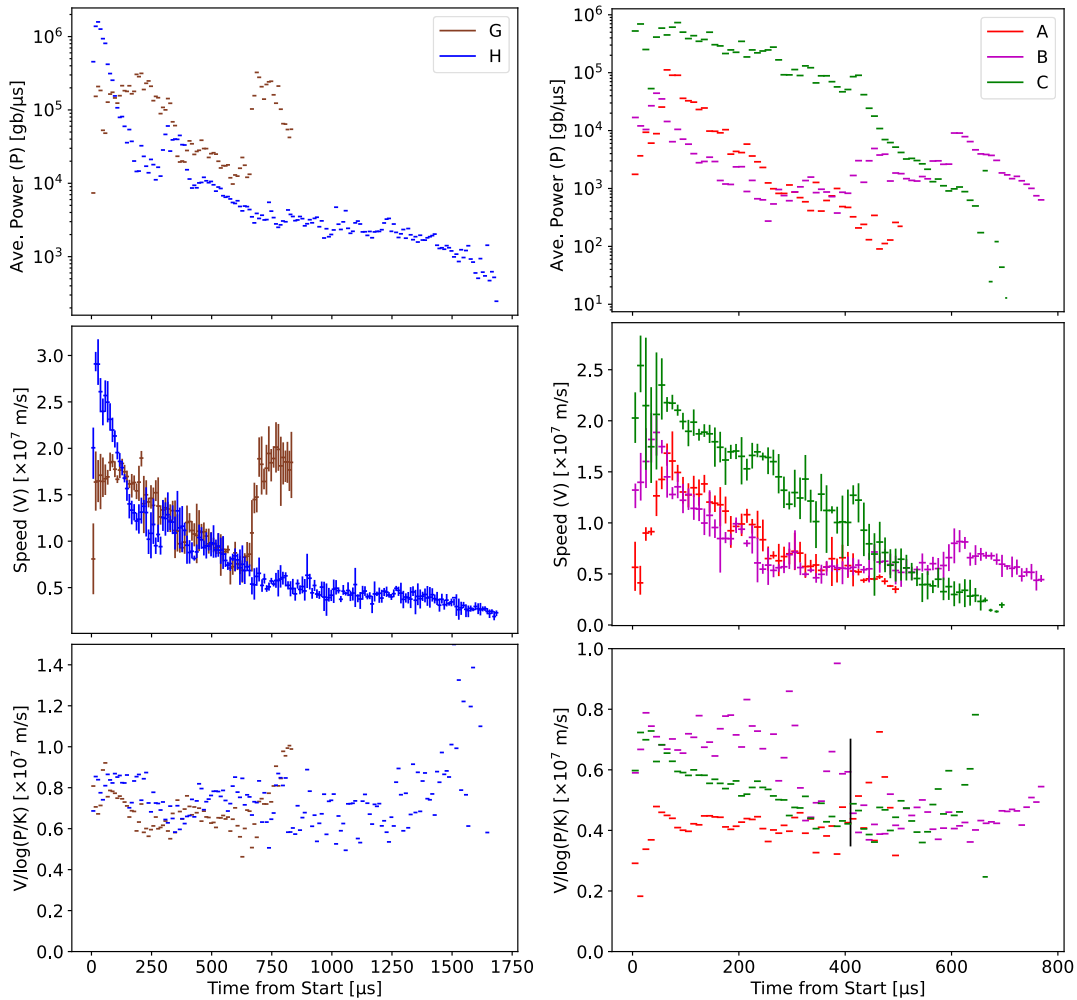


FIG. 6. Average power, average speed (bars show 16th and 84th percentile), and a log-linear ratio vs time for recoils G, H (left), and A, B, C (right). Width of lines shows duration of bins. Values of K are given in Table II. The right-hand figure shows a vertical bar which indicates a time that the behavior of recoil B changes significantly, discussed further in the text.

Figure 8 shows the speed and power for each recoil on a log-log scale. We choose a log-log scale for Fig. 8, as opposed to log-linear, to emphasize that the exponential relationship between power and speed suggested in Figs. 6 and 7 is not sacred. That is, the relationship between the power and speed is similar to, but not necessarily, exponential. In Fig. 8 recoil leaders A, C, and G are all very close to linear, ostensibly suggesting a power-law relationship between power and speed. Thus, Fig. 8 shows straight lines to indicate power-law fits per recoil, as defined by

$$P = \beta(V/10^7 \text{ m/s})^\alpha, \quad (5)$$

where β and α are constants that were found by fitting a line to $\log(P)$ and $\log(V)$ numerically, separately per recoil. The final values of β and α are shown in Table II, which demonstrates that the power-law index, α , changes significantly between the different recoil leaders. In addition, Table II shows that while β is in a similar range for all

recoils (around 10^4 gb/μs), it is significantly different. For example (as can be seen by eye in Fig. 8), recoil C is more intense than recoils A and B. However, the values in Table II should be treated with some skepticism, as it is not clear how they are affected by systematic effects such as imaging artifacts (for example, density of located sources).

Finally, recoil leaders B and H visibly differ from a power-law relationship between speed and vhf power. Recoil leader H clearly shows a banana like curve in Fig. 8, as if the power-law index changes smoothly over time. It should be noted that recoil H actually fits an exponential curve better than a power law, as can be seen by the fact that recoil H has a very flat $V/\log(P/K)$ in Figs. 6 and 7. Recoil leader B clearly shows a hook like shape in Fig. 8 around speed = 5×10^6 m/s, power = 10^3 gb/μs; indicated by a curving arrow in Fig. 8. This hook is the same change in P vs V behavior we discussed in reference to the exponential fit in Figs. 6 and 7. The sources in this hook occur after $T = 410 \mu\text{s}/D = 7.2$ km, as indicated by the vertical black line in Figs. 6

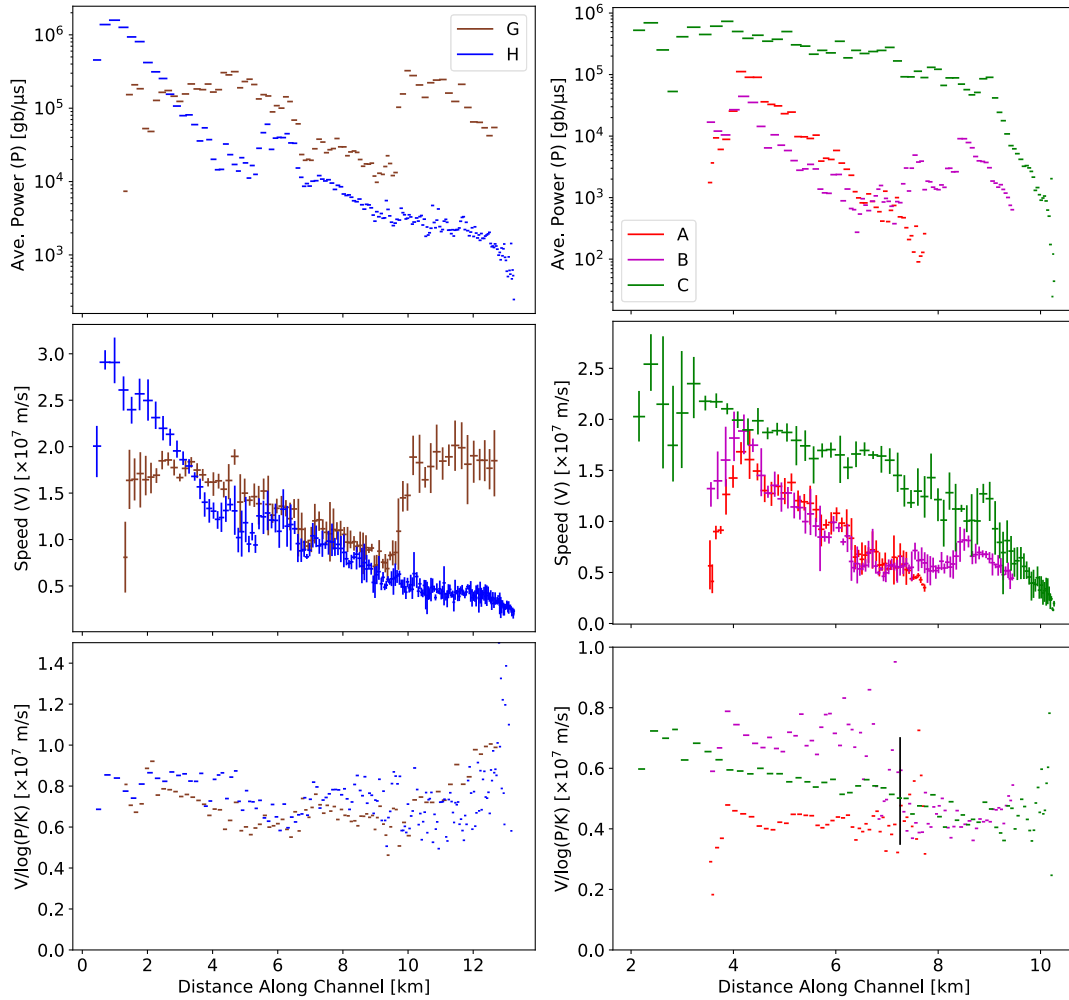


FIG. 7. Average power, average speed (bars show 16th and 84th percentile), and a log-linear ratio vs distance along the channel for recoils G, H (left), and A, B, C (right). Width of lines shows length of bins, and thus vary depending on the average speed. Values of K are given in Table II. The right-hand figure shows a vertical bar which indicates the location that the behavior of recoil B changes significantly, discussed further in the text. The vertical black bar is equivalent to the one in Fig. 6.

and 7. It is as if recoil leader B follows one relationship between speed and power for the first half of its lifetime, and then switches to a different relationship. Since recoils B and H do not truly match a power-law relationship, the error bars reported in Table II for recoil leaders B and H are likely significantly underestimated.

TABLE II. Exponential and power law results for five recoils, as defined by Eqs. (4) and (5). Uncertainties are 1 standard deviation errors as derived from the linear fits.

Recoil	Q [$\times 10^7$ m/s]	\log_{10} ($K/\text{gb}/\mu\text{s}$)	α	\log_{10} ($\beta/\text{gb}/\mu\text{s}$)
A	0.41 ± 0.02	1.3 ± 0.6	4.1 ± 0.2	3.81 ± 0.05
B	0.68 ± 0.03	2.0 ± 0.6	2.8 ± 0.2	3.55 ± 0.04
C	0.54 ± 0.02	2.3 ± 0.6	3.4 ± 0.1	4.61 ± 0.02
G	0.70 ± 0.05	2.9 ± 1.0	3.0 ± 0.2	4.47 ± 0.03
H	0.76 ± 0.01	2.7 ± 0.2	2.6 ± 0.1	4.28 ± 0.02

Figures 6–8 demonstrate that there is a close relationship between power and speed that is similar to either a power law or exponential relationship, but the exact nature of this relationship changes between different recoil leaders (even on the same channel), and a recoil leader can even change this behavior in the middle of its lifetime.

B. Small-scale intensity fluctuations

In this section we will show two examples of small-scale intensity fluctuations. The first is from recoil G, and is shown in Fig. 9; which also shows later recoil H at the same location. For comparison to Figs. 6 and 7 the location shown in Fig. 9 is about 1.7 km along the lightning channel, 38 μs after start of recoil G and 53 μs after start of recoil H. The dot size in Fig. 9 indicates source intensity. This figure shows that recoil G has about a 1.5 μs period where the source intensity decreases significantly. Fortunately there are still, weak, vhf sources located on the lightning channel

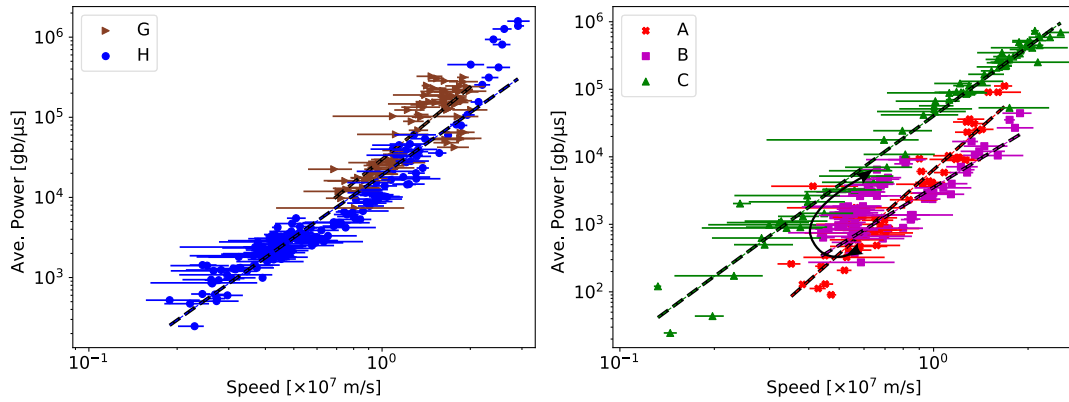


FIG. 8. Average power versus average speed (bars show 16th and 84th percentile) on a log-log scale. The line with arrow heads on the right indicate the hook in recoil B’s P vs V behavior.

during this period, which both shows that this effect is not a data-processing artifact of merely not locating sources and also allows us to measure the propagation speed during this intensity fluctuation. Figure 9 also shows that recoil H, which propagates over the same spot 32 ms later, does not show the effect to the same extent.

Figure 10 shows a set of time series data around the time of this intensity fluctuation for recoil G, and the time when recoil H propagates over the same spot. $T = 0$ is chosen as the time when the recoil passes over the center of the intensity fluctuation, indicated by a vertical bar. The top two panels show altitude of the vhf sources vs time, and recoil speed (derived from spline) averaged over each

spline knot. The reason for the average is that the spline cannot reproduce high-order behavior (e.g., stepping) inside the time of one knot, and therefore the precise speed vs time as extracted from the spline fit should be viewed with skepticism when analyzed on the timescale of individual knots (simply put: splines assume a certain level of smoothness, and therefore will not reproduce small-scale non-smooth behavior). Therefore, we only plot the average speed per knot to avoid over interpretation of the results. It should be noted that these small sections show no indication of stepping. The error bars of the speed are 1 standard deviation statistical uncertainties derived with a Monte Carlo technique. The third panel in Fig. 10 shows reconstructed

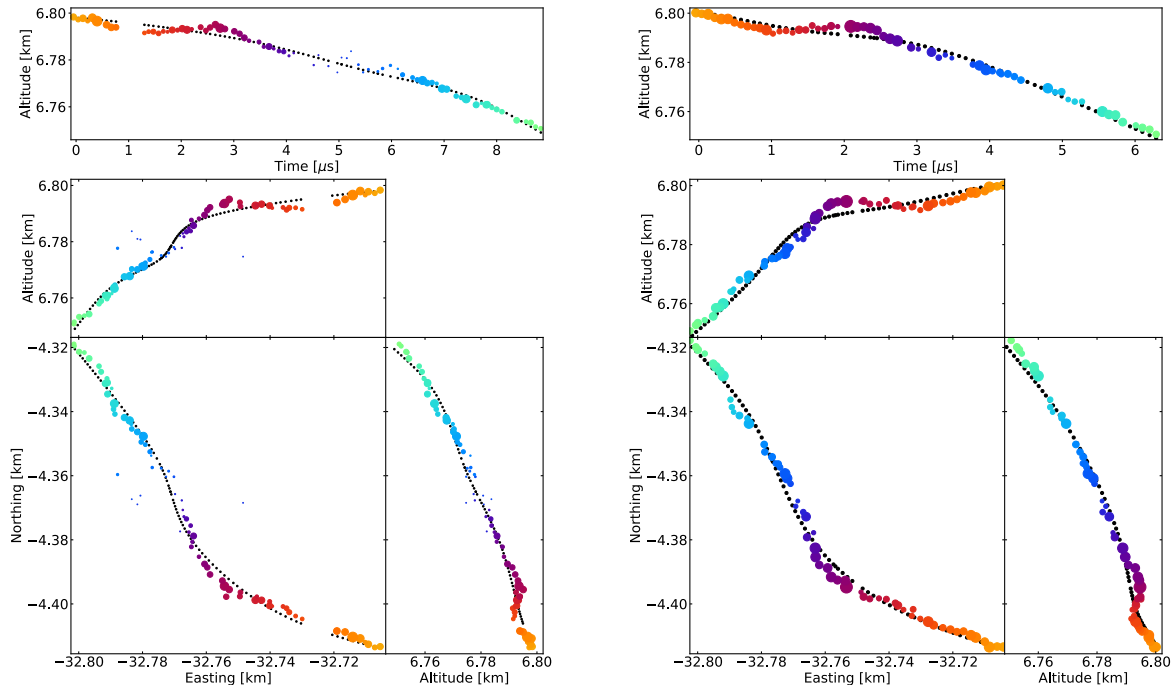


FIG. 9. Left: a small section of recoil G that shows a fluctuation in vhf intensity; $T_0 = 1125.14$ in Figs. 1 and 2. Right: a section of recoil H at the same spot; $T_0 = 1157.02$ in Figs. 1 and 2. T Dot size indicates source intensity. Color indicates time. Black dots spline fit.

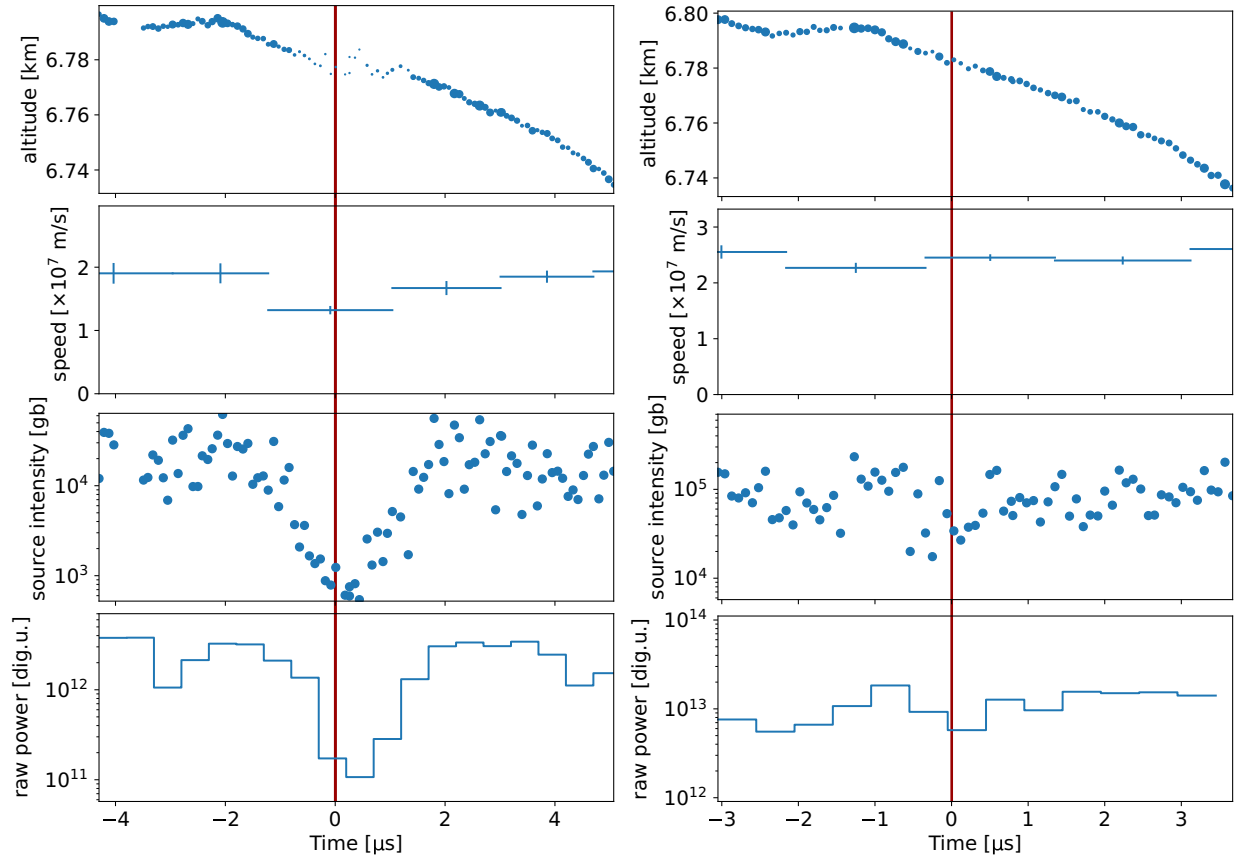


FIG. 10. Data during the intensity fluctuation of recoil G. $T = 0$ is when each recoil passes over the same location and is indicated by a vertical bar. Left: recoil G about $38 \mu\text{s}$ after start of recoil. Right: recoil H about $53 \mu\text{s}$ after start of recoil. Location is about 1.7 km along the lightning channel. Top: altitude of each radio source. Dot size indicates intensity. Second panel: leader speed averaged over spline knot. Error bar is 1 standard deviation uncertainty. Third panel: Imaged source intensity. Bottom: raw vhf power averaged over $0.5 \mu\text{s}$ bins, time aligned to the sources in middle panel, as received by a reference antenna in digitizer units (dig.u.).

source power from the imager; which involves beamforming, accounting for distance from the antennas, source dipole orientation, integration over 100 ns , and source cuts, and thus is not necessarily proportional to received antenna power. Therefore, the final panel shows raw vhf power (after RFI cleaning, see Sec. II) observed by a central antenna averaged over $0.5 \mu\text{s}$ bins. This raw antenna power has minimal processing, thus was included to demonstrate that the fluctuations in reconstructed source intensity are real and not imager artifacts. Note that the radio intensity is orders of magnitude above background, thus the statistical error bars on intensity are negligible.

Figure 10 demonstrates that the imaged intensity fluctuation clearly shows in the raw data for recoil G, but that recoil H definitely does not have a similar fluctuation. It is interesting to note that recoil G shows a small fluctuation in the speed at about the same time as the intensity fluctuation.

Figure 11 shows the time-series data similar to Fig. 10, of a second example of a small-scale fluctuation in recoil source intensity. In this case both recoil A and recoil B (about 21 ms after recoil A) show a significant drop in intensity as they propagate by the same location (aligned to

be at $T = 0$, indicated by a vertical bar). Note that the source intensity of recoil leaders A and B drop about 1 order of magnitude, while the drop in raw power is significantly less. This difference is likely due to the fact that there are negative leaders propagating at the same time as recoil leaders A and B (but no negative leaders during recoil leaders G, H, or C). For comparison to Figs. 6 and 7 the location shown in Fig. 11 is about 4.5 km along the lightning channel, $92 \mu\text{s}$ after start of recoil A, and $64 \mu\text{s}$ after the start of recoil B.

The two recoil sections shown in Fig. 11 do not show any statistically significant drop in speed at the same time as the drop in intensity. The section of recoil leader B in Fig. 11 is slowing down over time and does have a decrease in speed at $T = 0$ in Fig. 11; however this decrease in speed is about the same scale as the one standard deviation error bars, and thus is not statistically significant. Unfortunately, the error on the average speed in Fig. 11 is quite large (due to larger radial scatter in these two recoil sections), therefore it is entirely possible that there was a decrease in speed at the same time as the drop in intensity and is not evident in the data.

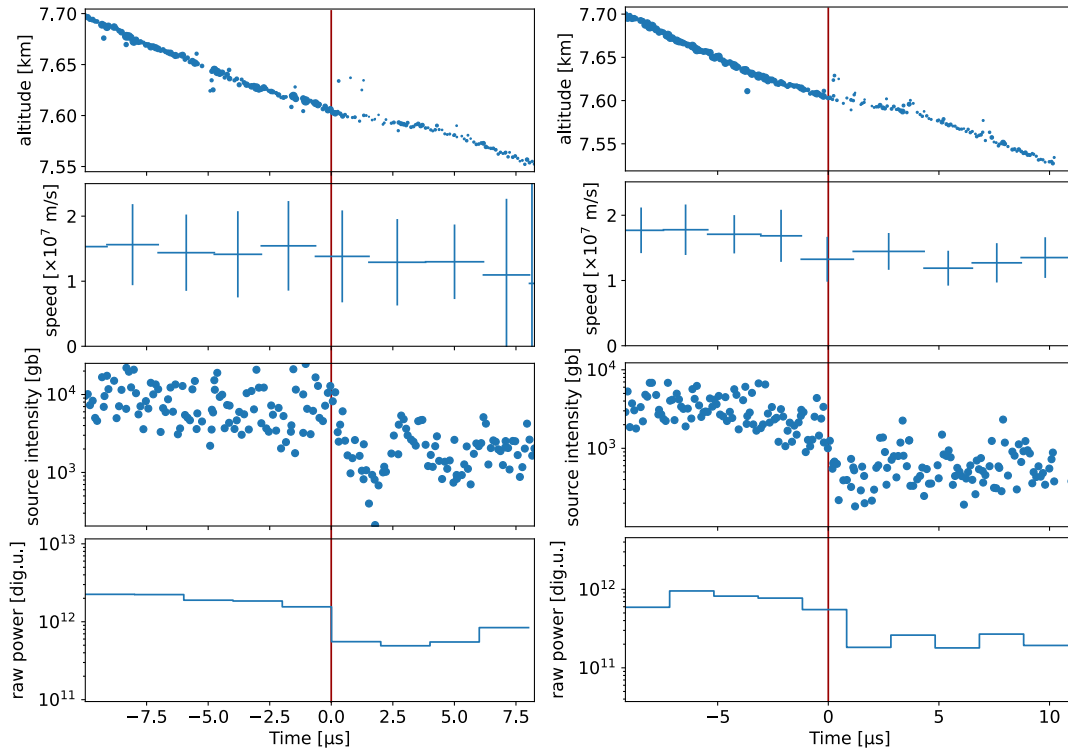


FIG. 11. Data during the intensity fluctuation of recoils A and B. $T = 0$ is when each recoil passes over the same location, and is indicated by a vertical bar. Left: recoil A about $92 \mu\text{s}$ from start of the recoil. Right: recoil B about $64 \mu\text{s}$ from start of the recoil. Location is about 4.5 km along the lightning channel. Top: altitude of each radio source. Dot size indicates intensity. Second panel: leader speed averaged over spline knot. Error bar is 1 standard deviation uncertainty. Third panel: Imaged source intensity. Bottom: raw vhf power averaged over $2 \mu\text{s}$ bins, time aligned to the sources in middle panel, as received by a reference antenna in digitizer units (dig.u.).

These two examples firstly show that recoils sometimes, if not often, have microsecond-scale vhf intensity fluctuations that are not related to stepping. The example in Fig. 11 persists between recoils A and B, and thus shows that these fluctuations are most likely some property of the plasma channel as opposed to the recoil wave. This property, however, can disappear as the channel ages.

IV. DISCUSSION AND CONCLUSION

In this work we have shown significant amount of data pertaining to recoil propagation. In summary we have observed the following:

- (1) Recoil leader channels have widths smaller than our resolution.
- (2) Recoil leaders have meter-scale tortuosity.
- (3) Recoil vhf intensity tends to decrease over time.
- (4) However, recoil vhf intensity does not just decrease, but may sometimes increase as well.
- (5) Changes in recoil vhf intensity can occur at the same location with subsequent recoils.
- (6) However, subsequent recoils can also have very different vhf intensities and speeds.
- (7) Fluctuations in recoil vhf intensity is strongly linked to propagation speed.

Creating a coherent explanation for all these observations is extremely challenging. We would expect that important recoil-propagation factors can be split into two broad categories; properties of the recoil wave, and properties of the underlying channel. Since the underlying channel typically is not actively undergoing dielectric breakdown by the time of recoil leader, we expect it can be described by having a width and a fraction of ionization. The recoil wave we expect to be solely described by charge.

The fact that recoils can be vhf thin, and that it is believed that vhf emission is due to streamer activity [2,20,21], indicates that recoil leader propagation involves significant streamer activity inside the leader core or at most inner portion of the corona sheath. If there is streamer activity in the corona region outside roughly 1 m radius it must be very vhf weak. One possibility is that since positive streamers initiate more easily than negative streamers [22,23], it may be reasonable to expect recoil propagation to be dominated by positively charged streamers. In this case the streamers would initiate in front of the recoil wave inside the ionized channel core, and propagate back towards and then connect with the recoil wave. This naturally explains both why there is weak streamer activity in the corona sheath, and why the recoil propagation emits significant vhf power (possibly due to either the positive

streamers initial acceleration or connection with the recoil front).

In this simple mental model recoil leaders exist as a pocket of charge that is carried forward by streamer activity in the leader core. In this context the recoil vhf power should be roughly proportional to (charge-per-streamer \times number-streamers \times peak-charge-acceleration)². While the recoil propagation speed should be roughly proportional to current, which is charge-per-streamer \times number-streamers \times average-streamer-speed. Thus, the relationship between vhf power and propagation speed of recoil leaders is already close to a power law with an index of 2; however, it also depends on the relationship between average streamer speed and peak charge acceleration. If the vhf emission is primarily due to streamer acceleration, then peak charge acceleration should just be the same as peak streamer acceleration. The other option is if vhf emission is due to streamer collisions [20] (e.g., if propagation is due to positive streamers that connect with the recoil wave), then the peak charge acceleration should be proportional to the duration of streamer collision processes. Therefore, however the vhf emission process occurs, it is likely that vhf emission and propagation speed are closely related simply because both are a result of streamer processes. However, without a better understanding of streamer physics it is difficult to comprehend why the relationship between vhf power and propagation speed of recoil leaders takes on a form that loosely resembles a power law/exponential relationship.

We expect the amount of charge in the recoil leader to decrease as the recoil propagates as charge is deposited in the leader corona sheath, and thus the speed and vhf intensity should decrease over time; which we do roughly observe. However, we also observe that recoil leaders can accelerate/increase intensity. This is difficult to understand under our model, as it ostensibly requires the recoil leader to pick up more charge, and it is difficult to think of a mechanism where a recoil leader could increase its charge. One option could be if the recoil leader connects with a leader branch with a more negative potential than the recoil leader. However, in this case we would expect the potential of the leader branches to equalize, thus only occur once. Figure 7, however, shows that recoils A and B both accelerate in the same location. The key to understand why recoil leaders can accelerate may come from the fact that we clearly observe that the plasma structure of the channel is important. This is clearly seen in Fig. 11 where recoil leaders A and B show the same dip in intensity at the same location. This can also be roughly seen in Figs. 6 and 7, which show that recoil leaders A and B have very similar shapes in speed and intensity when lined up as a function of distance but not as a function of time. The fact

that the structure of leader plasma is important could explain why recoil leaders accelerate. If the leader core is thinner, then the electric field will be higher for the same amount of charge, causing the recoil to propagate faster and emit more vhf radiation. (Note that since the channel core is only centimeters in size we do not expect to be able to directly measure any changes in its width.)

We believe that our observations provide strong constraints to future recoil leader modeling, and thus progress our understanding of the behavior of lightning plasma. Since our TRI-D interferometry inherently accounts for and extracts the 3D polarization of the vhf emission, we are planning on investigating the polarization of these five recoil leaders. Based on our observations that recoil leaders are vhf thin, we predict that recoil leaders emit vhf from their core, as opposed to corona sheath, and thus we expect the vhf polarization to be parallel to the channel propagation. This is different than a previous observation [24], which observed recoil vhf emission polarized perpendicular to propagation. In addition, in future work we would like to compare the negative leaders that preceded these recoil leaders in order to investigate if the recoil properties at all correlate with any original negative leader properties.

The data are available from the LOFAR LTA, see [25] [section “Staging Transient buffer Board (TBB) data”] for access. The file names of the flash data is [26]. Where “stat” should be replaced with the station name: CS001, CS002, CS003, CS004, CS005, CS006, CS007, CS011, CS013, C017, CS021, CS024, CS026, CS028, CS030, CS031, CS032, CS101, CS104, RS106, CS201, RS205, RS208, RS210, CS301, CS302, RS305, RS306, RS307, RS310, CS401, RS406, RS407, RS409, CS501, RS503, RS508, or RS509.

ACKNOWLEDGMENTS

The LOFAR cosmic-ray key science project acknowledges funding from an Advanced Grant of the European Research Council (Grant No. FP/2007-2013)/ERC Grant Agreement No. 227610. The project has also received funding from the European Research Council (ERC) under the European Union’s Horizon 2020 research and innovation programme (Grant Agreement No. 640130). B. M. H. is supported by NWO (VI.VENI.192.071) and ERC Grant Agreement No. 101041097. LOFAR, the Low Frequency Array designed and constructed by ASTRON, has facilities in several countries that are owned by various parties (each with their own funding sources), and that are collectively operated by the International LOFAR Telescope foundation under a joint scientific policy.

- [1] J. R. Dwyer and M. A. Uman, The physics of lightning, *Phys. Rep.* **534**, 147 (2014).
- [2] B. M. Hare *et al.*, Radio Emission Reveals Inner Meter-Scale Structure of Negative Lightning Leader Steps, *Phys. Rev. Lett.* **124**, 105101 (2020).
- [3] O. Scholten *et al.*, Distinguishing features of high altitude negative leaders as observed with LOFAR, *Atmos. Res.* **260**, 105688 (2021).
- [4] H. E. Edens, K. B. Eack, W. Rison, and S. J. Hunyady, Photographic observations of streamers and steps in a cloud-to-air negative leader, *Geophys. Res. Lett.* **41**, 1336 (2014).
- [5] S. Heckman, Why does a lightning flash have multiple strokes?, Ph.D. thesis, Massachusetts Institute of Technology, USA, 1992, p. 134.
- [6] D. P. Jensen, R. G. Sonnenfeld, M. A. Stanley, H. E. Edens, C. L. da Silva, and P. R. Krehbiel, Dart-leader and k-leader velocity from initiation site to termination time-resolved with 3d interferometry, *J. Geophys. Res.* **126**, e2020JD034309 (2021).
- [7] D. M. Jordan, V. P. Idone, V. A. Rakov, M. A. Uman, W. H. Beasley, and H. Jurenka, Observed dart leader speed in natural and triggered lightning, *J. Geophys. Res.* **97**, 9951 (1992).
- [8] M. G. Stock, M. Akita, P. R. Krehbiel, W. Rison, H. E. Edens, Z. Kawasaki, and M. A. Stanley, Continuous broadband digital interferometry of lightning using a generalized cross-correlation algorithm, *J. Geophys. Res.* **119**, 3134 (2014).
- [9] V. A. Rakov, M. A. Uman, K. J. Rambo, M. I. Fernandez, R. J. Fisher, G. H. Schnetzer, R. Thottappillil, A. Eybert-Berard, J. P. Berlandis, P. Lalande, A. Bonamy, P. Laroche, and A. Bondiou-Clergerie, New insights into lightning processes gained from triggered-lightning experiments in Florida and Alabama, *J. Geophys. Res.* **103**, 14117 (1998).
- [10] B. Hare *et al.*, Needle-like structures discovered on positively charged lightning branches, *Nature (London)* **568**, 360 (2019).
- [11] Y. Pu and S. A. Cummer, Needles and lightning leader dynamics imaged with 100–200 MHz broadband VHF interferometry, *Geophys. Res. Lett.* **46**, 13556 (2019).
- [12] M. Saba, A. de Paiva, and L. Concollato, Optical observation of needles in upward lightning flashes, *Sci. Rep.* **10**, 17460 (2020).
- [13] B. M. Hare *et al.*, Needle propagation and twinkling characteristics, *J. Geophys. Res.* **126**, e2020JD034252 (2021).
- [14] M. P. van Haarlem *et al.*, LOFAR: The low-frequency array, *Astron. Astrophys.* **556**, A2 (2013).
- [15] B. M. Hare *et al.*, LOFAR lightning imaging: Mapping lightning with nanosecond precision, *J. Geophys. Res.* **123**, 2861 (2018).
- [16] O. Scholten, B. M. Hare, J. Dwyer, N. Liu, C. Sterpka, S. Buitink, T. Huege, A. Nelles, and S. ter Veen, Time resolved 3d interferometric imaging of a section of a negative leader with LOFAR, *Phys. Rev. D* **104**, 063022 (2021).
- [17] O. Scholten, B. M. Hare, J. Dwyer, N. Liu, C. Sterpka, I. Kolmašová, O. Santolík, R. Lán, L. Uhlíř, S. Buitink, T. Huege, A. Nelles, and S. ter Veen, Interferometric imaging of intensely radiating negative leaders, *Phys. Rev. D* **105**, 062007 (2022).
- [18] K. Mulrey, A. Bonardi, S. Buitink, A. Corstanje, H. Falcke, B. Hare, J. Hörandel, T. Huege, P. Mitra, A. Nelles, J. Rachen, L. Rossetto, P. Schellart, O. Scholten, S. ter Veen, S. Thoudam, T. Trinh, and T. Winchen, Calibration of the LOFAR low-band antennas using the galaxy and a model of the signal chain, *Astropart. Phys.* **111**, 1 (2019).
- [19] O. Scholten *et al.*, The initial stage of cloud lightning imaged in high-resolution, *J. Geophys. Res.* **126**, e2020JD033126 (2021).
- [20] F. Shi, N. Liu, J. R. Dwyer, and K. M. A. Ihaddadene, VHF and UHF electromagnetic radiation produced by streamers in lightning, *Geophys. Res. Lett.* **46**, 443 (2019).
- [21] L. D. Boggs, D. Mach, E. Bruning, N. Liu, O. A. van der Velde, J. Montanyá, S. Cummer, K. Palivec, V. Chmielewski, D. MacGorman, and M. Peterson, Upward propagation of gigantic jets revealed by 3D radio and optical mapping, *Sci. Adv.* **8**, eabl8731 (2022).
- [22] N. Liu, B. Kosar, S. Sadighi, J. R. Dwyer, and H. K. Rassoul, Formation of Streamer Discharges from an Isolated Ionization Column at Subbreakdown Conditions, *Phys. Rev. Lett.* **109**, 025002 (2012).
- [23] J. Koile, F. Shi, N. Liu, J. Dwyer, and J. Tilles, Negative streamer initiation from an isolated hydrometeor in a subbreakdown electric field, *Geophys. Res. Lett.* **47**, e2020GL088244 (2020).
- [24] X.-M. Shao, C. Ho, M. Caffrey, P. Graham, B. Haynes, G. Bowers, W. Blaine, B. Dingus, D. Smith, and H. Rassoul, Broadband RF interferometric mapping and polarization (BIMAP) observations of lightning discharges: Revealing new physics insights into breakdown processes, *J. Geophys. Res.* **123**, 326 (2018).
- [25] https://www.astron.nl/lofarwiki/doku.php?id=public:lta_howto.
- [26] [srm://srm.grid.sara.nl/pnfs/grid.sara.nl/data/lofar/ops/TBB/lightning/L703974_D20190424T194432.504Z_“stat”_R000_tbb.h5](https://srm.grid.sara.nl/pnfs/grid.sara.nl/data/lofar/ops/TBB/lightning/L703974_D20190424T194432.504Z_“stat”_R000_tbb.h5).